Toxicology and Applied Pharmacology 459 (2023) 116357

Contents lists available at ScienceDirect

Toxicology and Applied Pharmacology

journal homepage: www.elsevier.com/locate/taap

Physiologically based modelling of dermal absorption and kinetics of consumer-relevant chemicals: A case study with exposure to bisphenol A from thermal paper

Barbara Wiśniowska [a], Susanne Linke [b,c], Sebastian Polak [a,d], Zofia Bielecka [a,d], Andreas Luch [b,c], Ralph Pirow [b,*]

[a] Faculty of Pharmacy, Jagiellonian University Medical College, Medyczna 9 Street, 30-688 Kraków, Poland
[b] German Federal Institute for Risk Assessment (BfR), Department of Chemical and Product Safety, Max-Dohrn-Straße 8-10, 10589 Berlin, Germany
[c] Department of Biology, Chemistry, Pharmacy, Institute of Pharmacy, Freie Universität Berlin, Berlin, Germany
[d] Simcyp Division, Certara UK Limited, Level 2-Acero, 1 Concourse Way, Sheffield S1 2BJ, UK

ARTICLE INFO

Editor Name: Lawrence Lash

Keywords:
Dermal absorption
Mechanistic modelling
Physiologically based toxicokinetic modelling
PBPK modelling
Dermal exposure
Bisphenol A

ABSTRACT

Bisphenol A (BPA) is one of the best studied industrial chemicals in terms of exposure, toxicity, and toxicokinetics. This renders it an ideal candidate to exploit the recent advancements in physiologically based pharmacokinetic (PBPK) modelling to support risk assessment of BPA specifically, and of other consumer-relevant hazardous chemicals in general. Using the exposure from thermal paper as a case scenario, this study employed the multi-phase multi-layer mechanistic dermal absorption (MPML MechDermA) model available in the Simcyp® Simulator to simulate the dermal toxicokinetics of BPA at local and systemic levels. Sensitivity analysis helped to identify physicochemical and physiological factors influencing the systemic exposure to BPA. The iterative modelling process was as follows: (i) development of compound files for BPA and its conjugates, (ii) setting-up of a PBPK model for intravenous administration, (iii) extension for oral administration, and (iv) extension for exposure *via* skin (*i.e.*, hand) contact. A toxicokinetic study involving hand contact to BPA-containing paper was used for model refinement. Cumulative urinary excretion of total BPA had to be employed for dose reconstruction. PBPK model performance was verified using the observed serum BPA concentrations. The predicted distribution across the skin compartments revealed a depot of BPA in the *stratum corneum* (SC). These findings shed light on the role of the SC to act as temporary reservoir for lipophilic chemicals prior to systemic absorption, which *inter alia* is relevant for the interpretation of human biomonitoring data and for establishing the relationship between external and internal measures of exposure.

Abbreviations: A, exposed skin area; ADAM, advanced dissolution, absorption and metabolism; ADME, absorption, distribution, metabolism, excretion; AUC, area under the concentration-time curve; BPA, bisphenol A; BPAG, glucuronidated BPA; BPAS, sulfated BPA; C_{max}, maximum concentration in plasma; D_{SCLip}, SC lipid diffusion coefficient; f_a, fraction absorbed; fu_{gut}, fraction of BPA unbound in the enterocyte; fu_{mic}, fraction unbound in microsomal incubation; fu_{sc}, fraction unbound in SC; GSA, global sensitivity analysis; IV, intravenous; IVIVE, *in vitro* to *in vivo* extrapolation; k_a, absorption rate constant; K_m, Michaelis-Menten constant; $Kp_{SCLip:Veh}$, SC lipid:vehicle partition coeffient; LSA, local sensitivity analysis; *m*, dose amount; MechDermA, mechanistic dermal absorption; MPML, multi-phase multi-layer; Q_{gut}, hybrid parameter of blood flow and compound permeability through enterocytes; QSAR, quantitative structure-activity relationship; *P*, octanol:water partition coefficient; P_{cell}, corneocyte permeability; PBPK, physiologically based pharmacokinetics; P1, P2, P3, P1-II, participant identifiers; *S*, solubility in the SSFL; SC, *stratum corneum*; SSFL, skin surface film liquid; SULT, sulfotransferase; UGT, UDP-glucuronosyltransferase; VE, viable epidermis; V_{max}, maximum velocity; Δx, thickness of the SSFL.

* Corresponding author at: Department of Chemical and Product Safety, German Federal Institute for Risk Assessment (BfR), Max-Dohrn-Straße 8-10, 10589 Berlin, Germany.

E-mail addresses: b.wisniowska@uj.edu.pl (B. Wiśniowska), susanne.linke@bfr.bund.de (S. Linke), sebastian.polak@uj.edu.pl (S. Polak), zofia.tylutki@uj.edu.pl (Z. Bielecka), andreas.luch@bfr.bund.de (A. Luch), ralph.pirow@bfr.bund.de (R. Pirow).

https://doi.org/10.1016/j.taap.2022.116357
Received 4 October 2022; Received in revised form 16 December 2022; Accepted 17 December 2022
Available online 23 December 2022

1. Introduction

Bisphenol A (BPA) is an estrogen-mimicking synthetic chemical (Krishnan et al., 1993; Shelby, 2008) that has come under intense scrutiny by regulatory agencies and academia due to concerns about potential health risks (Birnbaum et al., 2012; Schug et al., 2013; ECHA, 2015b; EFSA CEF Panel EFSA Panel on Food Contact Materials, Enzymes, Flavourings and Processing Aids, 2015; Heindel et al., 2015; ECHA, 2017a; ECHA, 2017b; EFSA, 2017). Consumers are exposed to BPA from multiple sources and *via* several routes. In its risk assessment from 2015, the European Food Safety Authority (EFSA) identified BPA-containing thermal paper as the source of second largest exposure (after diet), contributing around 10% to internal exposure to total (conjugated plus unconjugated) BPA in the general population (EFSA CEF Panel EFSA Panel on Food Contact Materials, Enzymes, Flavourings and Processing Aids, 2015; von Goetz et al., 2017). Since 2020, the use of BPA in thermal paper is restricted in the European Union (EC, 2016), after health risks for occupationally exposed people (*i.e.* cashiers) were identified by the European Chemicals Agency (ECHA, 2015b).

BPA has become one of the best studied industrial chemicals, not only in terms of toxicity but also in terms of toxicokinetics, that is, ADME (absorption, distribution, metabolism, excretion), and exposure. Given this wealth of information, the compound is an ideal candidate to exploit the recent advancements in physiologically based toxicokinetic (PBPK) modelling to better understand the dermal toxicokinetics of BPA specifically, and other consumer-relevant hazardous chemicals in general. This need is illustrated by EFSA's exposure assessment which concluded that the internal exposure to BPA *via* the dermal route was associated with a considerably higher degree of uncertainty than the one *via* the oral route (EFSA CEF Panel EFSA Panel on Food Contact Materials, Enzymes, Flavourings and Processing Aids, 2015; von Goetz et al., 2017). Using dermal exposure to BPA from thermal paper as a case scenario, the current study used mechanistic dermal absorption and PBPK modelling as a tool to improve internal exposure estimation.

The thermal paper basically consists of a base paper which is coated with a thermoreactive layer containing a colour-forming substance (*e.g.*, leuco dye) and a colour developer such as BPA, embedded in a binder matrix (Lassen et al., 2011; Mendum et al., 2011; ECHA, 2015a). Since BPA is not covalently bound to the matrix, it can be transferred to the skin during paper handling. The typical concentration of BPA for functional use in thermal paper is 1–3% (*w*/w) which relates to the weight of the finished product (Biedermann et al., 2010; Lunder et al., 2010; Schreder, 2010; Lassen et al., 2011; Liao and Kannan, 2011; Mendum et al., 2011; Geens et al., 2012; Danish EPA, 2014; Hormann et al., 2014; Eckardt and Simat, 2017). Expressed as load, *i.e.*, as mass of BPA relative to the surface area of thermal paper, average concentrations were reported to be 57 μg/cm^2 (Lassen et al., 2011), 94 μg/cm^2 (Hormann et al., 2014), and 80 μg/cm^2 (Eckardt and Simat, 2017).

Several studies measured the transfer of BPA from thermal paper to the skin (Biedermann et al., 2010; Schreder, 2010; Lassen et al., 2011; Danish EPA, 2014; Hormann et al., 2014; Eckardt and Simat, 2017). Biedermann et al. (2010) defined a standard scenario in which the BPA-containing side of thermal printing paper was pressed against the pads of the forefinger and the middle finger by the thumb for 5 s, applying a pressure as needed to pull the paper out of a printer. For slightly greasy skin (standard condition), the mean transfer on a single finger was 1.1 μg. For oily, humid, and wet fingers, average amounts of 6, 9, and 20 μg, respectively, were transferred. Further modifications involving a longer contact time (60 s) or repeated (3 or 10) contacts did not increase the amount of BPA transferred to the standard (slightly greasy) skin, suggesting that the skin surface film liquid (SSFL) was saturated in <5 s. Consistent with these results, Lassen et al. (2011) reported a mean transfer per finger pad of 1.8, 4.7, and 17 μg for dry, greasy, and humid conditions. Similarly, the Danish EPA (2014) reported values of 1.1, 3.2, and 17.7 μg/fingertip for dry, greasy, and humid conditions. Finally, Eckardt and Simat (2017) determined a mean BPA transfer per fingertip of ~0.4 and 43 μg, respectively, for dry and moist fingers. Assuming a contact surface area for a single fingertip/pad of 1–1.5 cm^2 (ECB, 2003; ter Burg et al., 2007; Bernier and Vandenberg, 2017), these transfer values translate into dermal loads of about 1 μg/cm^2 for the standard condition (dry to slightly greasy fingers) and 10–20 μg/cm^2 for a worst-case scenario (humid to wet fingers).

Information on dermal toxicokinetics of BPA in humans is available from a study involving the handling of simulated receipt paper (Liu and Martin, 2017) and from a study with the administration of BPA in different vehicles (ethanol, carboxymethylcellulose) to the volar forearm (Sasso et al., 2020). As the former study appropriately reflects realistic exposure scenarios with hand contact to thermal paper, it was used in the present study for PBPK model parametrization and verification.

Several PBPK models have been developed for BPA which include the dermal exposure route. Mielke et al. (2011) and Karrer et al. (2018) assumed that dermal exposure leads to a skin-surface depot, from which BPA enters the skin compartment according to donor-dependent first-order kinetics. Sharma et al. (2018) assumed the BPA to be deposited on the skin in a vehicle and modelled the transport based on the concentration difference between the skin surface and the skin compartment, the vehicle-to-skin partition coefficient, and a permeability rate constant. Sarigiannis et al. (2016) modelled the skin as a two-layer structure, covering the *stratum corneum* (SC) with its characteristic "bricks and mortar" structure and viable epidermis.

Except for the latter study, all other above-mentioned studies used a simple, two-compartment structure with first-order uptake kinetics to simulate the uptake of the chemical from the skin surface into the skin and further into the blood. While being easy to set-up and parametrize, these simple skin models can have limitations to reflect the complex and dynamic absorption phenomena following the short-term exposure to chemicals *via* hand contact. These phenomena include, *inter alia*, substance precipitation and dissolution on the skin surface, the occurrence of diffusionally induced time delays, and reservoir formation. If such phenomena are relevant, the simple models might not be able to capture the local and systemic kinetics of the substance.

The present study implements dermal absorption in a conceptually different way as we intended to model the absorption of BPA from thermal paper through hand skin layers with a refined approach which involves a mechanistically robust description of skin anatomy and physiology. The multi-phase multi-layer mechanistic dermal absorption (MPML MechDermA) model (Fig. 1) (Patel et al., 2022) available in the Simcyp Simulator was used to simulate the dermal toxicokinetics of BPA at local and systemic levels and to assess the role of physicochemical and physiological factors influencing the systemic exposure to BPA. Sensitivity analysis was conducted to quantify such correlations. Finally, the performance of the MPML MechDermA model was compared with that of a simpler (3-compartment) skin absorption model.

2. Methods

2.1. Model development

2.1.1. Study workflow

The study followed the general pattern of iterative (learn and confirm approach) model development and refinement as presented below and in Fig. 2. The main stages of the project were as follows:

1) Development and refinement of a PBPK model for BPA administered intravenously and for its main metabolites, BPA glucuronide (BPAG) and BPA sulfate (BPAS).
2) Extension of the developed PBPK model for orally administrated BPA and model verification.
3) Model extension for the dermal absorption of BPA.
4) Refinement and performance verification of the mechanistic PBPK model for dermal absorption of BPA against data from a dermal

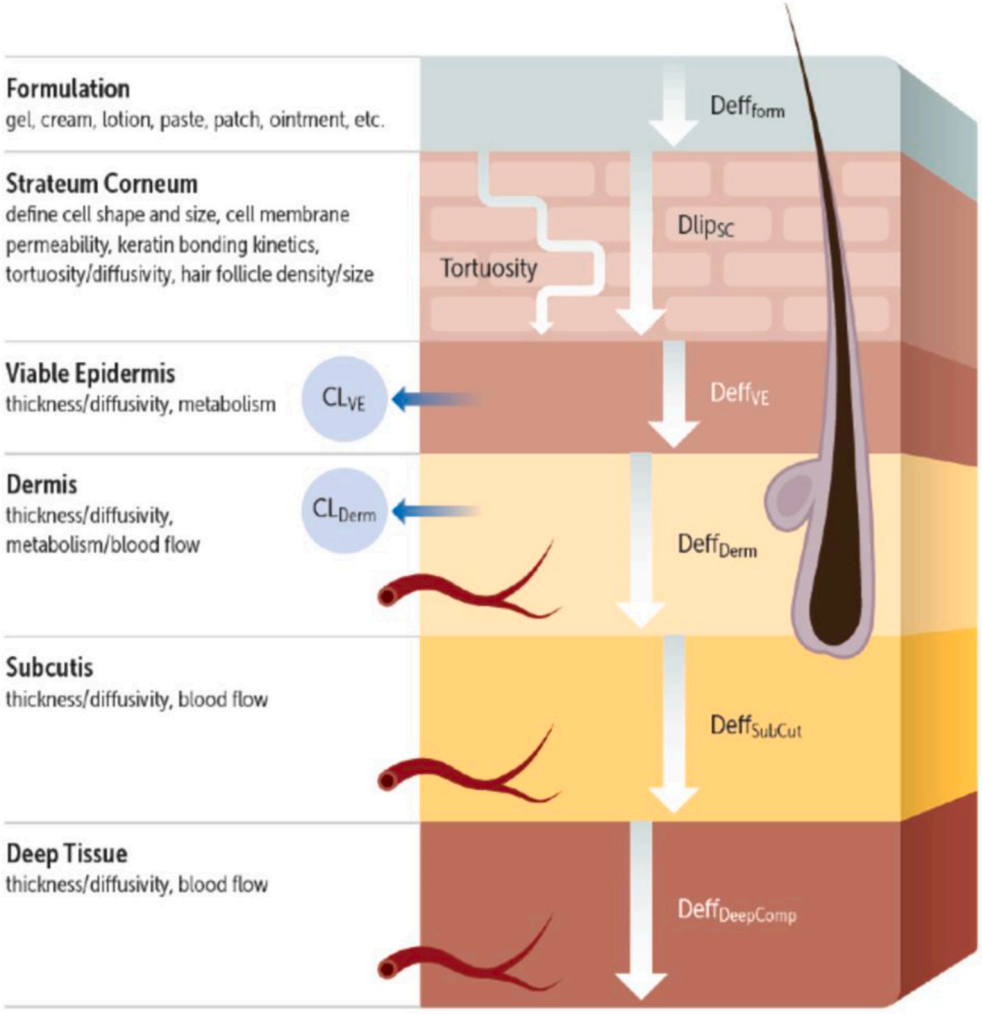

Fig. 1. Structure of the multi-phase and multi-layer (MPML) mechanistic dermal absorption (MechDermA) model showing the factors and variables that may impact absorption through each layer of the skin.

toxicokinetic study in humans involving the handling of simulated receipts containing isotope-labelled BPA (Liu and Martin, 2017).

All simulations were performed in Simcyp Simulator V21 (Certara UK, UK), which is a qualified platform for *in vitro* to *in vivo* extrapolation (IVIVE) and ADME data-based predictions of the toxicokinetics accounting for population variability (Jamei et al., 2013).

Data post-processing and visualization of the simulation outputs in Excel files were carried out in the statistical computing environment R (R Core Team, 2022) by use of the R packages readxl (Wickham and Bryan, 2022), lattice (Sarkar, 2008), and latticeExtra (Sarkar and Andrews, 2019).

2.1.2. *Intravenous and oral administration*

The first step of model building included the development of compound files for BPA, BPAG, and BPAS. Compound-related data necessary for building the PBPK model included relevant physicochemical and ADME information. The required physicochemical properties of BPA, BPAG, and BPAS, along with other compound-dependent parameters, were collected from the literature and databases, calculated in MarvinSketch 18.30.0 (http://www.chemaxon.com), or predicted by the use of Simcyp built-in QSAR models. Model parameter values for BPA, BPAG, and BPAS are published in our companion paper (Wiśniowska et al., 2022).

For BPA, we selected the full PBPK model, where all the major body organs and tissues are represented. The model was first set up for intravenous administration, and initial estimates for parameters related to volume of distribution and clearance were calibrated to fit the *in vivo* human data which was allometrically scaled from experimental data from several animal species (Cho et al., 2002). Renal clearance of BPA was parametrized based on toxicokinetic information taken from a clinical study with oral administration (Thayer et al., 2015). For BPAG and BPAS, the minimal PBPK model was chosen, where all tissues except liver and gut are lumped together as a single compartment (Chetty et al., 2018). Elimination of both conjugates *via* renal clearance was parametrized based on the data of Thayer et al. (2015).

Next, the model was extended to account for oral administration of BPA. Oral absorption was simulated by a first-order model implemented in Simcyp. Intestinal first-pass metabolism was accounted for by the Q_{gut} model (Yang et al., 2007; Yau et al., 2017). The Q_{gut} model predicts the fraction of BPA escaping gut metabolism; among its parameters the fraction of BPA unbound in the enterocyte (fu_{gut}) turned out to be sensitive (see Results and Discussion). Initial parameter estimates for the first-order absorption model were derived from the data of Thayer et al. (2015). This study was also used for model refinement, *i.e.* for the optimization of absorption and clearance parameters. Model performance verification for the oral route was carried out by simulating the clinical trials of Völkel et al. (2002) and Teeguarden et al. (2015). In each case, 10 virtual populations were simulated using the sample size, proportion of females, age range, and dose of the respective study

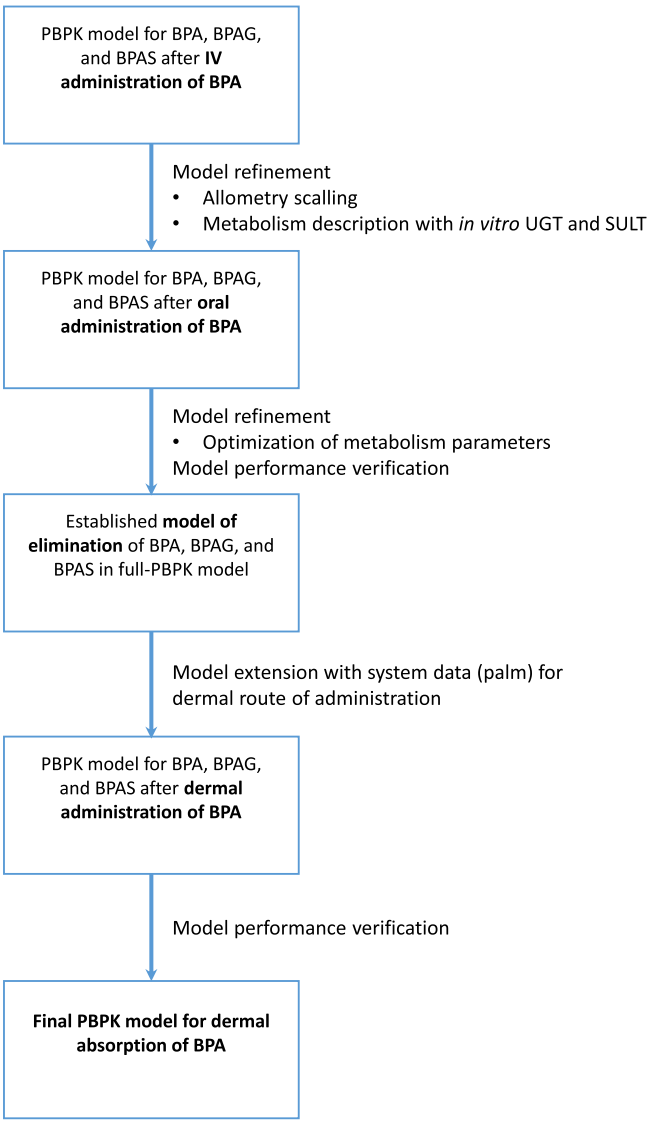

Fig. 2. Schematic overview of the workflow of the PBPK model development, refinement, and performance verification. BPAG, glucuronidated BPA; BPAS, sulfated BPA; IV, intravenous; UGT, UDP-glucuronosyltransferase.

populations. North European healthy volunteers' specific physiological parameters were used for all simulations. The details of all steps of modelling procedures and the final parameter estimates are described in our companion paper (Wiśniowska et al., 2022).

2.1.3. Dermal route of administration

The PBPK model was extended for the dermal route to simulate the exposure to BPA *via* hand contact. Parameters for the distribution, metabolism, and elimination processes were kept unchanged. The Simcyp MPML MechDermA model (Patel et al., 2015; Chetty et al., 2018; Puttrevu et al., 2020; Patel et al., 2022) was selected for the dermal absorption process (Fig. 1). Since the predefined application sites for this model do not include palmar skin, the skin morphology parameter settings for the inner (volar) forearm were selected as a base for subsequent adjustments. A literature search on palmar skin yielded 20 eligible papers with data on the number of SC layers, SC hydration levels, corneocyte dimensions, and the thickness of the main skin layers (see Supplementary data). Based on this data, skin morphology parameters were adjusted accordingly (Table 1). The hair follicle density was set to zero as human palm skin is devoid of hairs and sebaceous glands. The

Table 1
Skin morphology parameters of the MPML MechDermA Model with parameter values referring to the skin of the palm and front surface of fingers.

Parameter	Input value	Source
Skin temperature (°C)	32	Default value in Simcyp
Skin surface pH	4.5 / 5.2	Male / female
No. of SC layers	52	See Supporting information
Corneocyte thickness (μm)		
Top 25%	3.75	See Supporting information
Upper middle	3.90	Calculated in Simcyp from hydration level
Lower middle	4.10	and the density of water, SC lipids, SC
Bottom 25%	5.01	proteins (Nitsche et al., 2006)
Corneocyte width (μm)	25.2	See Supporting information
Corneocyte length (μm)	30.9	See Supporting information
Intercellular lipid thickness of SC (μm)	0.091	Default value in Simcyp
Tortuosity of the lipid diffusion pathway of SC	12.7	Default, from Talreja et al. (2001)
Hydration level (% water volume)		Egawa et al. (2007)
Top 25%	33	
Upper middle	36	
Lower middle	40	
Bottom 25%	57	
SC thickness (μm)	222	Value results from SC geometry
VE thickness (μm)	97.5	See Supporting information
Dermis thickness (μm)	746	Lee and Hwang (2002)
Hair follicle density (No./cm^2)	0	Palm skin has no hair follicle

Abbreviations: SC, *stratum corneum*; VE, viable epidermis.

lipid pathway tortuosity was kept at the default value which was derived from Talreja et al. (2001), who determined the lipid pathlength in the SC of human skin samples (back, abdomen, thigh) by microscopy techniques.

Skin physiology parameters describing the diffusion, partitioning, and protein binding were predicted by built-in QSAR models, except for the SC lipid:vehicle partition coefficient ($Kp_{SCLip:Veh}$), the SC lipid diffusion coefficient (D_{SCLip}), the corneocyte membrane permeability (P_{cell}), and the set of parameters related to subdermal tissue compartments (Table 2). The latter was kept at default values, which resulted in a negligible partitioning of BPA into the subcutis and subdermal muscle tissue due to the very small subcutis:dermis partition coefficient. P_{cell} was set to the lowest possible value to minimize the transfer of BPA into the corneocytes – a pragmatic decision to reduce model complexity. $Kp_{SCLip:Veh}$ and D_{SCLip} were obtained by optimization.

Skin physiology parameters related to the sebum compartment were not listed in Table 2 since they are not relevant in the palm-skin model which lacks hair follicles. The parameters related to the subcutis and subdermal muscle compartments, and also those related to keratin binding, were also not listed because there was virtually no partitioning into these compartments.

The toxicokinetic study of Liu and Martin (2017) was used for model refinement. The authors loaded soft notebook paper (6 cm × 10 cm) with deuterated BPA (d16-BPA, 20 mg) at a concentration of 2.5% (*w/w*) being comparable to that of native thermal paper. The BPA load (333 μg/cm^2) was 4–6-fold higher than in native thermal paper (see Introduction), because of the paper's higher grammage (*i.e.*, weight per area ratio). Six male participants handled the simulated thermal paper with one hand for 5 min and then put a nitrile glove on the exposed hand for 2 h. Between 0.02 and 0.87 μg d16-BPA was recovered afterwards from the exposed skin using water-moistened hand wipes. Serum concentrations of free and total d16-BPA (measured at three time points over 7.5 h post-dosing) were below the LOD of 0.061 nM. One participant underwent a second trial and then had detectable serum concentrations (measured at 22 h and 51 h post dose); 3 μg d16-BPA was recovered from his exposed hand. Cumulative urinary excretion of total BPA was not

Table 2
Skin physiology parameters of the MPML MechDermA model.

Parameter	Input value	Source
Partition coefficients		
SC lipid:Water	210.22	QSAR predicted (Nitsche et al., 2006)
SC lipid:Vehicle ($Kp_{SCLip:Veh}$)	40–392	Optimized (for $\Delta x = 50$ μm; see text)
SC lipid:VE	4.248	QSAR predicted (Shatkin and Brown, 1991)
Dermis:VE	0.139	QSAR predicted (modified Chen et al., 2015)
Dermis:Blood	2.738	QSAR predicted (Shatkin and Brown, 1991)
Subcutis:Dermis	1×10^{-6}	Default value in Simcyp
Diffusion coefficients (cm^2/h)		
Formulation/vehicle	0.0204	Predicted for water solution (Scheibel, 1954)
SC lipid (D_{SCLip})	1.28–7.50 × 10^{-6}	Optimized (see text)
VE	6.45×10^{-4}	QSAR predicted (modified Chen et al., 2015)
Dermis	6.45×10^{-4}	QSAR predicted (modified Chen et al., 2015)
Transfer into corneocytes		
Corneocyte membrane permeability (cm/h)	1×10^{-12}	Lower bound in Simcyp (quasi no permeation)
(Sub)Dermis binding		
Fraction unbound in dermis ISF	0.967	

Abbreviations: ISF, interstitial fluid; SC, *stratum corneum*; VE, viable epidermis; Δx, thickness of the SSFL.

quantifiable or very low (≤0.31 μg d16-BPA) in three of the first-trial subjects. We therefore decided to use the data of the other first-trial participants (P1, P2, P3) and from the second trial (P1-II) for PBPK model refinement.

Information on dermal dose (*i.e.*, the amount of BPA transferred from the paper to the skin) and exposed hand surface area was not available from Liu and Martin (2017). To tackle this problem, we took several values from a plausible range for each parameter (see Introduction for dermal dose and text below for skin surface area) and tested all combinations of parameter values. For each combination, the parameter estimation (PE) module in Simcyp Simulator was used to optimize $Kp_{SCLip:Veh}$ and D_{SCLip} so that the model predictions matched the observed cumulative urinary excretion of total BPA. An additional constraint was imposed on dermal dose by requiring the predicted amount of unabsorbed BPA to approach the amount recovered from the skin.

For the exposed skin surface area, we assumed values of 25 cm^2 (part of the palm plus 5 finger pads) (Bernier and Vandenberg, 2017) to 100 cm^2 (half of the inner hand surface area) (Table 3). The latter is a rounded-up value and was derived from men's inner hand surface area (*i.e.* palm plus the front surface of the fingers), which occupies 0.9% (Rhodes et al., 2013) of men's average total body surface area of 2 m^2 (Te Biesebeek et al., 2014). The dermal dose was varied such that the predicted amount of unabsorbed BPA was in the vicinity of the observed amount recovered from the skin.

From the different formulation types available for the MPML MechDermA model, we selected the suspension, since we assumed that BPA dissolves in the skin surface film liquid (SSFL) up to the solubility limit; the undissolved fraction was assumed to be in the solid phase as particles with a radius of 5 μm (default value). We used the solubility in water since human palm skin contains only eccrine glands, which secrete sweat consisting mostly of water and NaCl (Baker, 2019). The aqueous solubility of BPA at 25 °C was reported to be 0.12 and 0.30 mg/mL (EC, 2003). Li et al. (2007) measured 0.381 mg/mL at 25 °C and 0.466 mg/mL at 30 °C. Solubility values of 0.1 and 0.5 mg/mL were therefore selected to cover the uncertainty (Table 3). The thickness of the SSFL was assumed to range from 2 to 50 μm, thereby accounting for the uncertainty about the degree of sweat formation when trans-epidermal evaporative water loss is blocked by an occlusive glove. The upper bound is consistent with Jonathan (2008) who measured a sweat layer thickness of 59 μm on the palm following a 30-min period of occlusion by an experimental index matching fluid. The lower bound is twice the lowest possible value acceptable by the MPML MechDermA model.

Table 3
Trial design parameters of the clinical study with the dermal application (Liu and Martin, 2017).

Parameter	Input value	Source
Trial design		
Population	Healthy volunteers	
No. of trials	10	As in clinical trial
No. of subjects in trial	5	As in clinical trial
Age	25–35	
Proportion of females	0	As in clinical trial
Dose (mg)	0.002–0.021	See text
Application site	Palm and front surface of fingers	As in clinical trial
Duration of application (h)	2	As in clinical trial
Application area (cm^2)	25, 50, 100	See text
Formulation type	Suspension	See text
Thickness (μm)	2, 10, 50	See text
BPA solubility (mg/mL)	0.1, 0.5	See text
Particle radius (μm)	5	Default value in Simcyp

The uncertainties associated with the thickness of the SSFL and the solubility of BPA in the SSFL were additionally accounted for by parameter variation. This raised the number of exposure parameters to be varied from three to five, so that the total number of parameter combinations increased to 54. For each combination, the PE module in Simcyp Simulator was used to optimize $Kp_{SCLip:Veh}$ and D_{SCLip} so that the model predictions matched the observed cumulative urinary excretion of total BPA. As the software did not provide the option to get the sum amount of the parent compound and its metabolites, parameter optimization was based on matching the observed excretion of total BPA to the predicted excretion of the glucuronidated BPA (expressed as BPA equivalents). This pragmatic approach was regarded acceptable since 88% of the excreted total BPA was predicted to be glucuronidated. Therefore, no adjustment was applied to the optimized parameters.

Model performance verification for the dermal route was limited since the only toxicokinetic study by Liu and Martin (2017) involving palmar skin as application site was already used for model refinement and the optimization of skin physiology parameters. However, since it was only the cumulative urinary excretion profile that was employed for optimization, the serum concentrations of unconjugated and total BPA could be used for a partial performance verification.

2.1.4. Sensitivity analysis

The developed PBPK models involve a large number of input parameters. To identify which of the input parameters are most influential on the simulation outcome, we used a quantitative approach belonging to the local sensitivity analysis (LSA) methods (Loucks and van Beek, 2017). The approach consisted here in computing indexes reflecting the rate of change in the output summary parameters AUC and C_{max} induced by a defined variation in an input parameter around its initial (*i.e.*, nominal) value. Specifically, two indices, namely a sensitivity index and an elasticity index, were used.

The sensitivity index (*SI*) is used to measure the magnitude of change in an output variable Q per unit change in the magnitude of an input parameter P from its initial value P_0 (Loucks and van Beek, 2017). For a

change ΔP in the value of an input parameter P from its initial (nominal) value P_0, the sensitivity index can be calculated as:

$$SI = \frac{Q(P_0 + \Delta P) - Q(P_0 - \Delta P)}{2\Delta P}$$

The elasticity index (*EI*) is a dimensionless expression of sensitivity which measures the relative change in the output variable Q for a relative change in an input parameter P (Loucks and van Beek, 2017). This can be derived from the sensitivity index *SI* as:

$$EI = \frac{P_0}{Q(P_0)} SI$$

A relative change of 0.25 was chosen when varying an input parameter P from its initial value P_0 (*i.e.*, $\Delta P/P_0 = 0.25$). The only exception was fractional input parameters with a nominal value (and upper bound) of 1, for which a one-sided change (*i.e.*, decrease) by a relative change of 0.1 was chosen.

The LSA approach is able to capture the influence of local variations of selected input parameters on the variations of an output variable. However, insights on the impact of local variations on the variations of the output might not be sufficient to fully understand the determinants of the variations of the output variable. In this context, global sensitivity analysis (GSA) methods are valuable approaches, differing from LSA as they investigate the effects of the variations of selected parameters by exploring the whole parameter space and considering simultaneously the effects of interactions between parameters on the variations of the output variable (Sumner et al., 2012; Iooss and Lemaître, 2015). In addition to the implemented LSA, a GSA was therefore performed and applied to the most influential parameters identified by the LSA, with a focus on parameters related to dermal absorption. Among the available GSA techniques, we applied Morris' method using the mean of the absolute elementary effects as well as the Sobol method using the total effect index (Sumner et al., 2012; Iooss and Lemaître, 2015). The input parameters tested with GSA were ranked by order of influence on the output variable and were compared with the results of the LSA.

3. Results and discussion

3.1. Intravenous administration

The iterative model development and refinement process started with the simulation of an intravenous bolus injection. The simulation showed that the initial parameter estimates did not capture the systemic plasma clearance as predicted from allometric scaling (Wiśniowska et al., 2022). It turned out that the underprediction was caused by the IVIVE from the kinetic data of the recombinant human UDP-glucuronosyltransferases UGT1A9 and UGT2B15, which were identified by Street et al. (2017) as hepatic UGTs showing the highest BPA glucuronidation activity. The pragmatic solution to approach the target plasma clearance was to adjust the fraction unbound in the microsomal incubation (fu_{mic}). Virtually equivalent would have been a proportional adjustment of the Michaelis-Menten constants (K_m), or inverse proportional adjustments of the maximum velocity (V_{max}) values or the recombinant human UGT tissue scalars, since the tissue concentration of unbound BPA for relevant doses ($\leq$100 μg/kg BW) would be far below the K_m values of both UGTs. A tissue scalar puts the expression and activity of the native enzyme in the tissue of interest in relation to that of the recombinant enzyme in the *in vitro* system (Gibson et al., 2013). The outcome of the local sensitivity analysis (see below) reflects the equivalence of these adjustments.

Under-predictions of intrinsic tissue/organ clearance (and in consequence systemic clearance) by IVIVE is not an unexpected finding for UGTs; many factors have been identified which could potentially contribute to an under-prediction of human clearance for UGT substrates (Hutzler and Zientek, 2016). These factors include, *inter alia*, the influence of incubation conditions, dependence on a consistent purified enzyme source, lack of an easy method to quantify UGT abundance; lack of specific substrates to establish relative activity factors for IVIVE, and the release of free fatty acids from the microsomal membrane that are potent inhibitors of certain UGTs.

3.2. Oral route of administration

The toxicokinetic study of Thayer et al. (2015) with administration of 100 μg/kg BW of d6-BPA in a cookie was used for refining the PBPK model for the oral route. Running the PBPK model with the initial parameter estimates for the first-order absorption model and the Q_{gut} model revealed an over-prediction of the BPA plasma level. The model refinement involved the increase of fu_{gut} to the recommended value of 1 (Yang et al., 2007; Yau et al., 2017) and the adjustment of the absorption rate constant (k_a). Final refinement steps comprised the adjustment of hepatic sulfation clearance and the renal clearance of BPAS. The final parameter estimates are provided in the companion paper (Wiśniowska et al., 2022).

Fig. 3 shows the corresponding model predictions for the refined parameter setting. Overall, there was a good agreement between the observed data and the predicted plasma levels and cumulative urinary excretions of BPA, BPAS, BPAG, and total BPA. The model predictions showed some deviations from the observed plasma concentration-time profiles in the first hours post-dosing for BPA and BPAG as well as in the terminal phase for BPAG (Fig. 3B/D). Deviations were also noted for total BPA, but these were mainly caused by the deviations in the plasma level of BPAG, which contributes most to total BPA. The difficulty to capture the initial time course of BPA and BPAG is explained by the limitations of the first-order absorption model and the Q_{gut} model, which are not able to reflect the more complex physiological processes such as active transport across the apical and basolateral membranes, and the differential regional expression of intestinal enzymes and transporters. There is evidence from *in vitro* studies suggesting that intestinal transporters are involved in the BPA efflux from the enterocytes back into the gut lumen and in the basolateral transport of BPAG into the portal blood (Yoshikawa et al., 2002; Mazur et al., 2012).

The advanced dissolution, absorption and metabolism (ADAM) module of Simcyp (Jamei et al., 2009) would in principle be able to cover these complex physiological processes. However, adequate quantitative *in vitro* data are lacking which prevent a parametrization of active transport. Nevertheless, switching on the ADAM module without active transport improved the agreement for BPA and BPAG (see Wiśniowska et al., 2022), which suggests that regional physiological intestine parameters like blood flow are relevant parameters contributing to the specific shape of the plasma concentration profiles in the first hours post-dosing. As regards the terminal phase, BPAG is predicted to be cleared much faster than what is observed. This phenomenon was already noted by Yang et al. (2015) who described it as lingering of serum BPAG levels (and BPA levels) at later time points, and they explained it by the enterohepatic recirculation of BPAG. By assuming a fraction of BPAG to be secreted into the gut through the bile duct, Yang et al. (2015) were able to simulate this peculiar behaviour. With the ADAM model, by attributing a certain portion of the systemic (*i.e.*, renal) clearance of BPAG to biliary clearance, and by additionally enabling the back-conversion of BPAG into BPA in the gut lumen, it is possible to simulate this behaviour (Wiśniowska et al., 2022).

The cumulative urinary excretion was well predicted for BPA, BPAG, and total BPA. The coefficient of variation of 20% (default: 30%) for the fraction absorbed (f_a) was chosen well, as it captured the variability in the cumulative urinary excretion of total BPA at 24 h post-dose (gray-shaded area in Fig. 3E). The cumulative urinary excretion of BPAS at 24 h post-dose was, however, overpredicted by a factor of 3.6. We could adjust the renal clearance for BPAS to match the cumulative urinary excretion, but this would have introduced a mismatch in the plasma concentration-time profile of BPAS (Fig. 3C). Accordingly, we can only acknowledge a certain degree of toxicokinetic inconsistency between

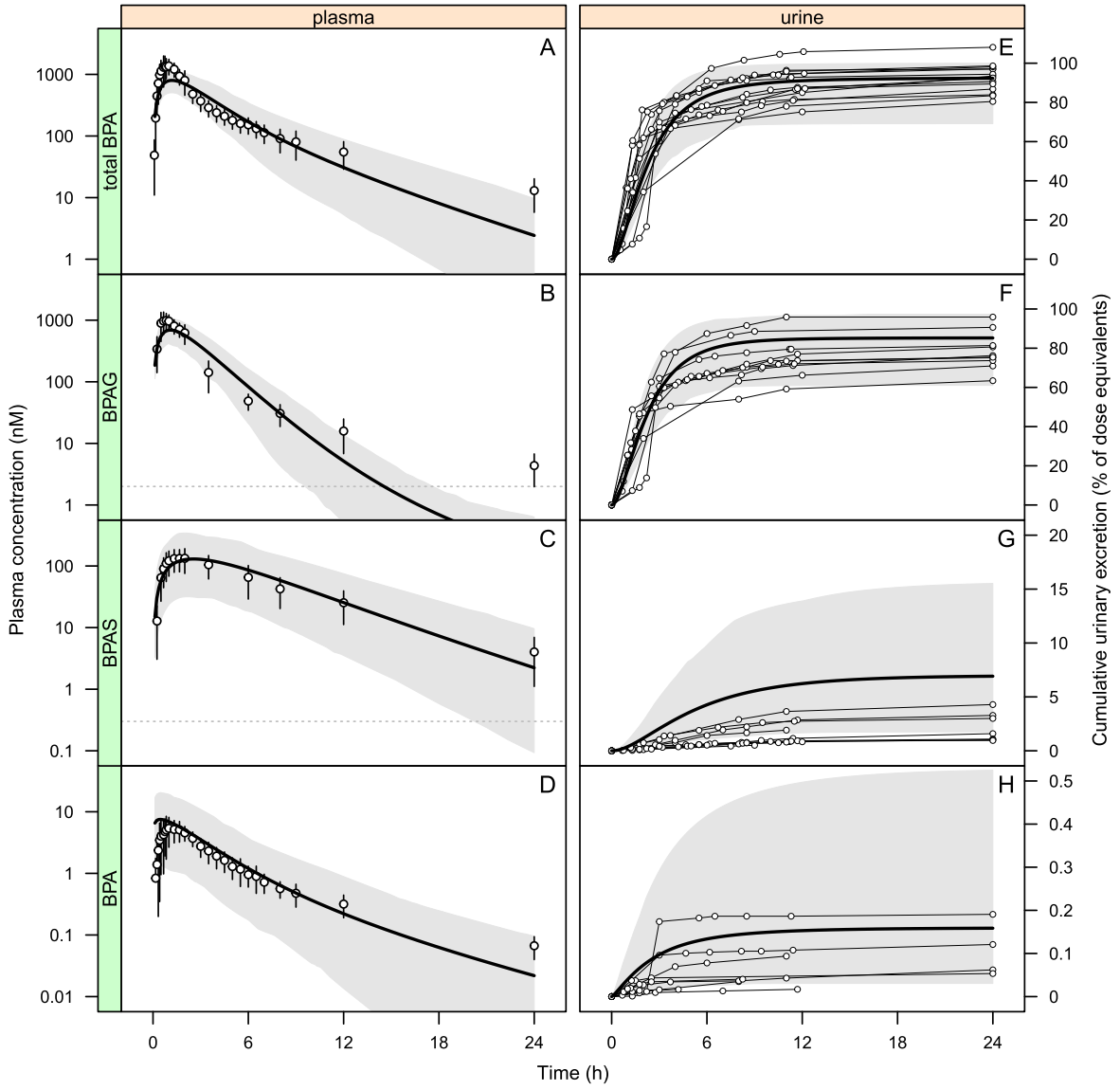

Fig. 3. Predicted and observed plasma/serum concentration-time profiles and cumulative urinary excretion profiles of unconjugated, sulfated (BPAS), glucuronidated (BPAG), and total BPA following oral dosing of deuterated BPA. PBPK model predictions show the population means (black solid lines) and the 5th to 95th percentile range (gray-shaded area). Circle symbols with error bars represent the mean ± standard deviation of the observed serum concentrations from the toxicokinetic study of Thayer et al. (2015). Circle symbols connected by lines show the observed individual cumulative urinary excretions. The subjects ingested the deuterated BPA in a cookie at a dose of 0.1 mg/kg BW. Dashed lines indicate the limit of detection (LOD).

the observed plasma and urine data for BPAS.

A local sensitivity analysis (LSA) was performed to identify which input parameters were most influential on the simulation outcome. Using the AUC and C_{max} for the BPA plasma concentration as output summary parameters, and the elasticity index as a normalized sensitivity measure, the following input parameters were identified as most influential: fraction (of BPA) unbound in plasma, UGT-related parameters, and the oral absorption parameters (Wiśniowska et al., 2022). This result points towards the critical importance of plasma binding for toxicokinetic processes of BPA distribution and elimination. It also stresses the importance of high-quality and reliable *in vitro* metabolism data for IVIVE. Regarding the AUC for the plasma concentration of BPAG and BPAS, the renal clearance was the most sensitive input parameter; an elasticity index of −1 was obtained for both compounds, indicating that an increase in CL_{renal} causes a decrease in AUC of the same relative magnitude.

Two studies were identified and used for the model performance verification (Völkel et al., 2002; Teeguarden et al., 2015). The simulation and verification results are presented in Fig. 4. Völkel et al. (2002) administered 5 mg d16-BPA in a gelatine capsule and measured the plasma concentration of unconjugated and glucuronidated BPA. The plasma concentration of BPA was below the limit of detection (LOD) of 10 nM, consistent with our model prediction (Fig. 4A). The simulated plasma concentration of BPAG agreed well with the observed data over the initial post-dosing period but showed the expected under-prediction in the terminal phase.

In the study of Teeguarden et al. (2015), volunteers ingested a tomato soup containing 0.03 mg/kg BW of d6-BPA. The predicted plasma concentrations of BPAG and total BPA showed the expected outcome, *i.e.*, an agreement with the observed data during the initial phase and an under-prediction in the terminal phase (Fig. 4C). An unexpected over-prediction was obtained for BPA and BPAS. The downslope of BPAS plasma concentration was overpredicted by a factor of 2.9, being of similar magnitude as the over-prediction of cumulative urinary excretion of BPAS in Thayer et al. (2015). To reduce the over-prediction, a more extensive clearance of BPA towards the glucuronide, either pre-

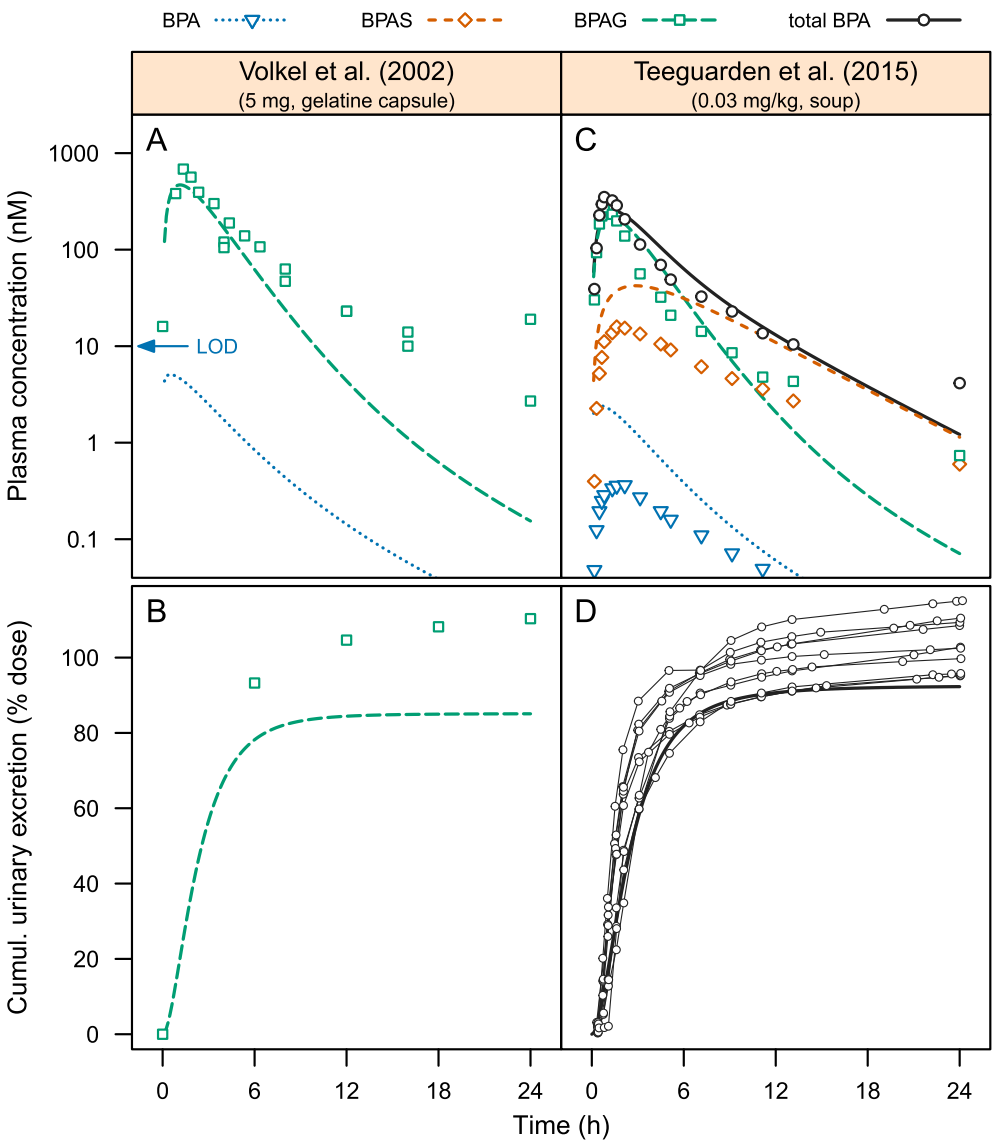

Fig. 4. Predicted and observed plasma/serum concentration-time profiles and cumulative urinary excretion profiles of unconjugated, sulfated (BPAS), glucuronidated (BPAG), and total BPA for two toxicokinetic studies with oral dosing of deuterated BPA. Thick (solid, dashed, and dotted) lines show the population means of the PBPK model predictions. Unconnected circle symbols show the observed mean values and connected circle symbols the individual cumulative urinary excretions from the toxicokinetic studies (Völkel et al., 2002; Teeguarden et al., 2015). Doses and dosage forms are indicated.

systemically or systemically, or both, would be required.

To sum up, based on the studies of Völkel et al. (2002) and Teeguarden et al. (2015), the model performance for the oral route was considered satisfactory. A further model refinement at this stage was not needed.

3.3. Dermal route of administration

The PBPK model was extended to accommodate the exposure to BPA *via* hand contact. The data of the first-trial and second-trial subjects (P1, P2, P3, P1-II) participating in the dermal toxicokinetic study of Liu and Martin (2017) were used for model refinement. Lack of information on dermal dose and exposed hand surface area made it necessary to use dose reconstruction from urinary excretion for model refinement. The uncertainty associated with dermal dose, exposed hand surface area, and with two further exposure-related parameters, the thickness of the skin surface film liquid (SSFL) and the solubility of BPA in the SSFL, were accounted for by parameter variation. For each combination, the parameter estimation module in Simcyp Simulator was used to optimize the SC lipid:vehicle partition coefficient ($Kp_{SCLip:Veh}$) and the SC lipid diffusion coefficient (D_{SCLip}) so that the model predictions matched the observed cumulative urinary excretion. An additional constraint was imposed on dermal dose by requiring the predicted amount of unabsorbed BPA to approach the amount recovered from the skin.

Parameter estimation was performed for the representative of the virtual healthy volunteer population and with the data of the first-trial and second-trial subjects (P1, P2, P3, P1-II). The optimization of $Kp_{SCLip:Veh}$ and D_{SCLip} revealed that a continuum of combinations of exposure-related parameter values was compatible with the observed urinary data of an individual experiment. This was reflected by the coincidence of the predicted excretion profiles for all 54 combinations (Supplementary Fig. S1). The optimized D_{SCLip} for each subject was virtually the same for all combinations. This parameter was therefore kept fixed at the subject-specific optimized value when re-running the parameter estimation for $Kp_{SCLip:Veh}$. Across all subjects and trials, the optimized value for D_{SCLip} ranged from 1.28 to 7.50 $\times$ 10^{-6} cm^2/h (Supplementary Fig. S2).

The plausible range for the dermal dose could be narrowed so that model predictions matched the observations for both the cumulative urinary excretion and the unabsorbed amount. For the first-trial subjects (P1, P2, P3), plausible dermal doses were in the range of 2–5 μg (Supplementary Fig. S2). For the second-trial subject (P1-II), a considerably higher value of 20 μg was obtained. It needs to be considered, however, that the actual values for the unabsorbed amount (and consequently for

the dermal dose) could have been higher, as information on any residual BPA possibly adhering to the glove was not reported. Another aspect is that the systemic circulation is the only sink in the MPML MechDermA model for BPA deposited in the skin. In reality, in the several days after taking off the occlusive glove from the subject's exposed hand, additional removal processes such as dermal contact with other surfaces, skin washing, and desquamation very likely resulted in a transfer of BPA from the exposed skin to the environment. Thus, a BPA amount higher than predicted would need to enter the skin to still match the cumulative urinary excretion when these additional removal processes are to be considered.

The optimized $Kp_{SCLip:Veh}$ varied largely, depending on the parameter combination (Fig. 5). When applying the upper values for exposed skin area ($A = 100$ cm^2) and solubility ($S = 0.5$ mg/mL), the increase in the SSFL thickness (Δx) from 2 μm to 50 μm resulted in a proportional increase in the optimized $Kp_{SCLip:Veh}$. The reason for this is clear: the increase in SSFL thickness enlarged the SSFL volume which in turn decreased the BPA concentration in the SSFL (provided the concentration is always below the solubility limit). The impact of the increased SSFL thickness on diffusive mass transfer was negligible, as the diffusion coefficient for the SSFL was four orders of magnitude higher than D_{SCLip} (Table 2), rendering the transport from the SSFL into the SC a non-rate-limiting step in the diffusion cascade from SSFL to blood. Thus, a given fold decrease in BPA concentration was compensated by the same-fold increase in $Kp_{SCLip:Veh}$ to maintain the driving force for diffusion into the SC. The same explanation applies for the dependence of the optimized $Kp_{SCLip:Veh}$ on dermal dose (Fig. 5).

For the upper value of SSFL thickness ($\Delta x = 50$ μm), the optimized $Kp_{SCLip:Veh}$ became solely dependent on dermal dose, *i.e.*, independent on variations in exposed skin area and solubility; this was reflected by the coincidence of all curves in Fig. 5. Again, the reason is clear: first, the BPA concentration in SSFL remained always below the solubility limit, and second, any variation in exposed skin area resulted in a proportional change in SSFL volume, which in turn caused an inversely proportional change in BPA concentration. Since the diffusive mass transfer depends on the product of the area by the concentration, the reciprocal changes in both parameters cancelled out each other.

For a certain region of the explored parameter space (A, Δx, S, m), the optimized $Kp_{SCLip:Veh}$ did not depend on dose amount (m) and SSFL thickness (Δx), but instead changed in a proportional manner upon variation of the other two parameters. This occurred when Δx was reduced to 2 μm and was reflected by the vertical shift of the horizontal lines in Fig. 5. It resulted from quasi-infinite dose conditions, when the BPA was not completely dissolved in the SSFL so that the BPA concentration in the continuous phase was always at the solubility limit (Supplementary Fig. S3).

Model performance verification for the dermal route was performed using the serum concentrations of unconjugated and total BPA of the second-trial subject (P1-II). Simulations were conducted for the healthy, male volunteer population, using plausible values for the exposure-related parameters (*e.g.*, dermal dose of 20 μg) and the optimized skin-physiology parameters (Fig. 6). The pre-check of the cumulative urinary excretion of total BPA confirmed the slight overprediction (Fig. 6C) already known from simulations for the population representative. The predicted mean plasma concentration for total BPA agreed with the observed serum concentrations measured at 22 h and 51 h post

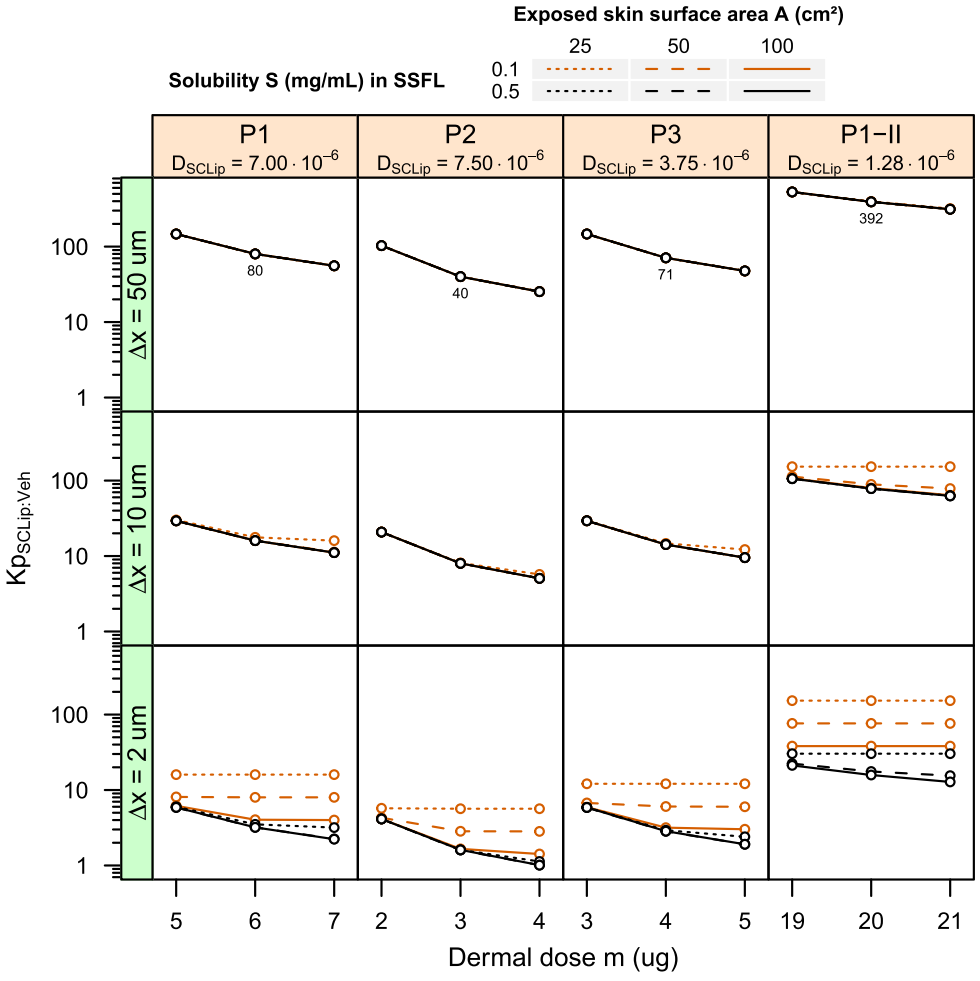

Fig. 5. Optimized SC lipid:vehicle partition coefficient ($Kp_{SCLip:Veh}$) in relation to dermal dose (m), exposed skin surface area (A), BPA solubility (S) in the skin surface film liquid (SSFL), and SSFL thickness (Δx). The columns of this two-dimensional matrix plot show the optimized $Kp_{SCLip:Veh}$ determined for the first-trial and second-trial subjects (P1, P2, P3, P1-II) participating in dermal toxicokinetic study of Liu and Martin (2017). $Kp_{SCLip:Veh}$ was optimized together with the diffusion coefficient in SC lipid (D_{SCLip}) to match the observed cumulative urinary excretion of total BPA for each study participant.

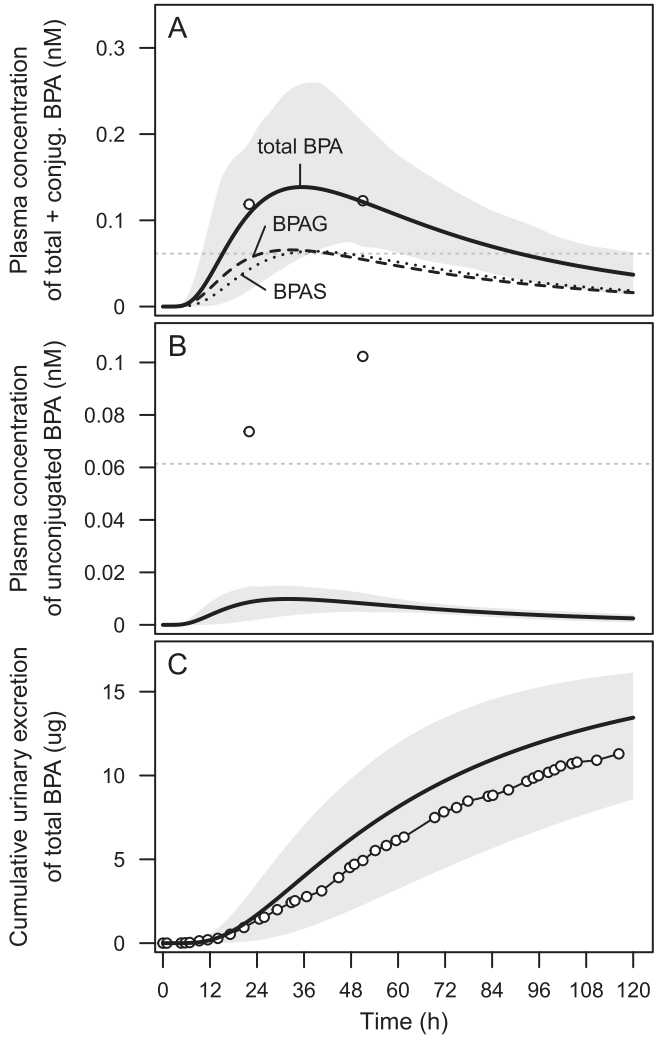

Fig. 6. Simulated plasma concentration-time profiles of unconjugated, conjugated (BPAG, BPAS), and total BPA as well as cumulative urinary excretion of total BPA following the dermal exposure to 20 μg BPA for 2 h. Model predictions are shown as population means (thick solid, dashed, and dotted lines) and 5th to 95th percentile ranges (gray-shaded areas). Simulations were performed for the healthy volunteer population (50 males, 25–35 years old) using an exposed skin surface area of 50 cm^2, a BPA solubility in the skin surface film liquid (SSFL) of 0.5 mg/mL, a SSFL thickness of 50 μm, and the optimized skin-physiology parameters ($D_{SCLip} = 1.28 \times 10^{-6}$ cm^2/h, $Kp_{SCLip:Veh} = 392$). Circles show the observed data for the second-trial subject (P1-II) of Liu and Martin (2017). Mass-based amounts refer to the normal (non-deuterated) BPA.

dose (Fig. 6A). Based on the population means for C_{max} and AUC, the conjugates BPAG and BPAS each accounted for 46% of the predicted plasma concentration of total BPA. The observed serum concentration for unconjugated BPA at 21 and 51 h grossly exceeded the predicted levels (Fig. 6B). Expressed as percentage of total BPA plasma concentration, the unconjugated BPA amounted to 62% and 84% in the study of Liu and Martin (2017) compared to the 7% in the simulation. We note that the predicted percentage is consistent with the experimental value of 8.81%, which was determined in a toxicokinetic study with dermal administration of BPA to the volar forearm (Sasso et al., 2020).

The simulated plasma concentration profile of total BPA showed a wide peak occurring more than one day after the 2-h dermal exposure (Fig. 6A). This response is in contrast to the early and sharp peak observed with oral dosing (Fig. 3A). The delayed peak concentration indicates the formation of a skin reservoir from which BPA is slowly released into the blood stream. The predicted distribution of BPA across the different skin compartments (Fig. 7) showed the largest percentage of dermal dose (20 μg for second-trial subject P1-II) to be in the SC. The preferential partitioning into the SC lipids in connection with the thickened SC (222 μm for the palms, see Table 1) explains the delayed transport of BPA into the viable epidermis, and then further *via* the dermis into systemic circulation. After five days (120 h), the SC still contained 13.4% of the dermal dose (Fig. 7). The predicted distribution of BPA across the SC layers revealed an initially steep inward gradient which progressively flattened over time following the cessation of exposure after 2 h (Supplementary Fig. S4).

An LSA was performed to identify which input parameters of the MPML MechDermA Model (Tables 1 and 2) were most influential on the AUC and C_{max} for the BPA plasma concentration used as output summary parameters (Supplementary Fig. S5). Based on the elasticity index, the following skin morphology parameters were identified as most influential (in decreasing order): number of SC layers, tortuosity of the lipid diffusion pathway in the SC, and the intercellular lipid thickness of the SC. Most influential among the skin physiology parameter was the

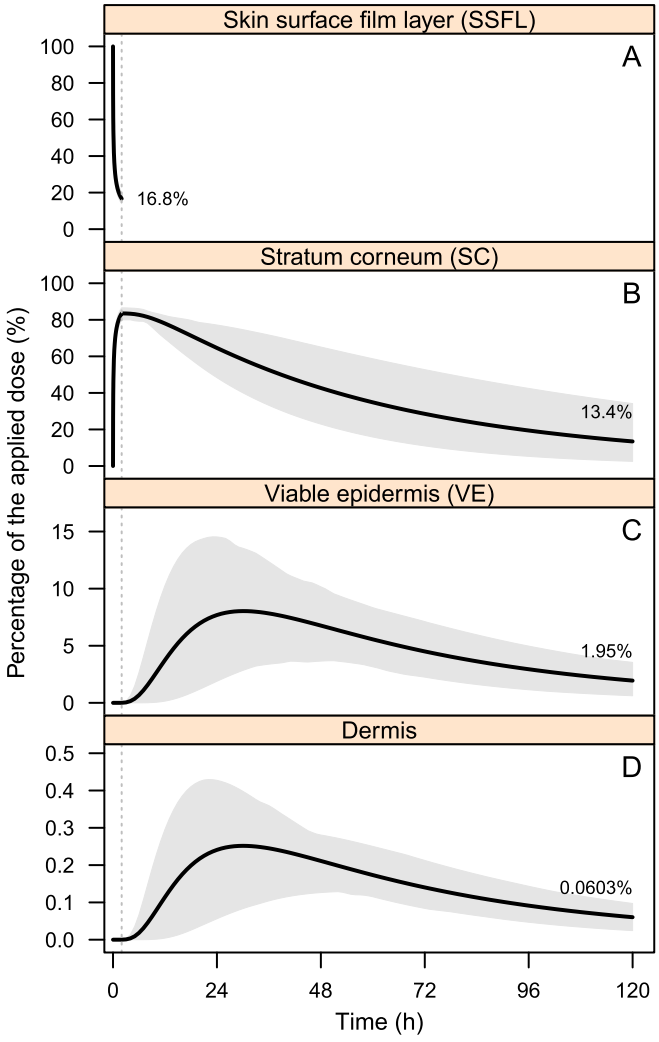

Fig. 7. Simulated time course of the percentage of the applied dose in different skin compartments following the dermal exposure to 20 μg BPA for 2 h. Model predictions are shown as population means (black solid lines) and 5th to 95th percentile ranges (gray-shaded areas). Simulations were performed for the healthy, male volunteer population. Dashed vertical lines indicate the end of dermal exposure at 2 h. Numbers show the percentage of the applied dose remaining in the respective compartment at the end of exposure (panel A) or after 120 h. For further information on trial-design parameters and optimized skin-physiology parameters, see Fig. 6.

SC lipid diffusion coefficient (D_{SCLip}), followed by the SC lipid:vehicle partition coefficient ($Kp_{SCLip:Veh}$).

In addition to the implemented LSA, a global sensitivity analysis (GSA) was performed and applied to the most influential parameters identified by the LSA, comprising all skin morphology parameter in Supplementary Fig. S5, the partition coefficients related to vehicle, SC, and viable epidermis, and the diffusion coefficients for SC lipids and viable epidermis. The tested input parameters were ranked by order of influence on the output variables. The results of the GSA confirmed in a qualitative manner the results drawn from the conducted LSA.

An additional parameter of potentially great influence was the corneocyte permeability (P_{cell}). This parameter describes the transfer from the SC lipid compartment into the corneocyte, which is assumed to be composed of a water and protein core encapsulated within a lipid envelope (Patel et al., 2022). The default setting is a P_{cell} value of 10^{-5} cm/h and steady-state binding to keratin, which is based on the fraction unbound in the SC (fu_{sc}). While fu_{sc} can be predicted by QSAR models, there is currently no method available to predict P_{cell}. We noticed that the default value for P_{cell} was associated with a very long time for distributing the BPA into the corneocyte and for reaching a dynamic equilibrium between the lipid and corneocyte compartments. As a pragmatic solution, P_{cell} was set to the lowest possible value of 10^{-12} cm/h to prevent a partitioning of BPA into the corneocytes.

We also analysed the model behaviour with P_{cell} set to 0.01 cm/h, for which the transfer step from the SC lipid compartment into the corneocyte is no longer rate limiting. Parameter fu_{sc} was 0.1515, predicted by a QSAR model (Polak et al., 2018). With this setting, the optimization of $Kp_{SCLip:Veh}$ and D_{SCLip} failed to yield model predictions that matched the observed cumulative urinary excretion of total BPA. In a next step, keratin binding was disabled by setting fu_{sc} to 1. With this setting, the matching between the predicted and observed data improved considerably but did not reach the goodness of fit of the setting with disabled partitioning into the cornecoyte. Compared to the latter, the optimized values were on average 8-fold lower for $Kp_{SCLip:Veh}$ and 20-fold higher for D_{SCLip}, and the derived dermal doses were 3–7 μg higher, reflecting a higher transfer of BPA from the SSFL into the skin. The lower optimized value for $Kp_{SCLip:Veh}$ resulted from the enabled partitioning of BPA into the corneocytes; the higher optimized value for D_{SCLip} was needed to keep the diffusion rate through the SC sufficiently high to capture the cumulative urinary excretion of BPA. However, the obtained $Kp_{SCLip:Veh}$ and D_{SCLip} values were not plausible as it turned out that the steady-state concentration in the SC lipid compartment equalled that of the corneocyte water compartment. An inspection of differential eq. 8 in Patel et al. (2022) revealed that the corresponding partition coefficient ($Kp_{SCLip:Water}$) is not included. Apart from this technical issue, additional experimental data from *e.g. in-vitro* skin permeation testing on the BPA content in the SC (ideally from tape-stripping) would be needed to clarify the possibility a partitioning of BPA into the corneocytes.

The optimized values for the SC lipid:vehicle partition coefficient ($Kp_{SCLip:Veh}$) and the SC lipid diffusion coefficient (D_{SCLip}) need some further discussion in terms of physicochemical and biological plausibility. The optimized $Kp_{SCLip:Veh}$ varied largely in the range of 1–530, depending on the choice of the exposure-related parameters, and on subject and trial. This parameter describes the concentration ratio of a substance between the vehicle and the SC lipids at equilibrium. A value of 1 would apply if SC lipids would have been used as vehicle, and a value of 210 for an aqueous vehicle (Table 2). Since the skin surface film liquid (SSFL) acted as a vehicle, and since eccrine glands of palm skin secrete aqueous sweat, $Kp_{SCLip:Veh}$ values in the range of 1–210 appear to be plausible. However, additional experimental data are needed to reduce this parameter uncertainty.

The optimized value for D_{SCLip} was in comparison to $Kp_{SCLip:Veh}$ in a narrower range of 1.28–7.50 $\times$ 10^{-6} cm^2/h, which also reflects the interindividual variability. However, it is important to precise that attributing these interindividual variations on D_{SCLip} to solely the interindividual variability on the SC lipid composition would be mistaken. This is because, for each individual, the parameter D_{SCLip} was estimated by matching the predicted cumulative urinary excretion evaluated for an "average subject" to the observed data for that considered individual. Predictions at the single "average" subject level are obtained using mean values of the PBPK model parameters calculated at the population level. However, at this population level, inter-individual variability in skin morphology and physiology parameters occurs and is simulated in Simcyp, with the exception of D_{SCLip}, and such variations affect the diffusive resistance of the skin. This cannot be reflected when optimizing the D_{SCLip} value for the average subject, so that the observed range of D_{SCLip} is thus the uncertainty in the value for the average subject.

The individuals' optimized values for D_{SCLip} were 2–14-fold lower than the default value of 1.76 $\times$ 10^{-5} cm^2/h predicted by a QSAR model (Mitragotri, 2003). This suggests that BPA diffuses more slowly through SC lipids than predicted. However, there is some uncertainty as to which extent the chosen values for the intercellular lipid thickness and tortuosity of the lipid diffusion pathway (Table 1), which were derived from thin and usually hairy, meshed skin, can be applied as well to the thick and hairless, ridged skin of the palmar surface of the hands. In addition, there is uncertainty on the partitioning of BPA into the corneocytes which can affect the estimation of D_{SCLip} (see above). The optimized values for D_{SCLip} should therefore be regarded as apparent values until the geometry of the SC lipid pathway is verified and the partitioning into the corneocytes is clarified, and further experience is gained from applying the MPML MechDermA Model to other experimental data.

The MPML MechDermA model was able to capture the delayed and long-lasting urinary excretion of total BPA following the exposure to BPA *via* hand contact. However, given the large number of skin parameters, the question arises as to whether such a model complexity is really needed, that is, whether this model is superior to simpler ones such as first-order or few-compartment models. To test the hypothesis of superiority, we switched to the simpler MechDermA model available in Simcyp Simulator while keeping the systemic part of the PBPK model exactly the same. The MechDermA model is based on the three compartmental (formulation/vehicle, SC and viable epidermis) model of Shatkin and Brown (1991) (Polak et al., 2012). The thickness of the three compartments was the same as in the MPML MechDermA model. The partition and diffusion coefficients were predicted by QSAR models, except for the SC:vehicle partition coefficient, the SC diffusion coefficient, and the viable-epidermis diffusion coefficient, which were optimized (Supplementary Table S1). It turned out that the MechDermA (3-compartment) model is not able to capture the time lag in and the shape of the urinary excretion profile of total BPA (Supplementary Fig. S6). This indicates that a more complex skin model with a multi-layer SC is needed to capture the transient diffusion processes in the SC which causes the delayed appearance of BPA in urine.

The lack of information on dermal dose and exposed skin surface area made it necessary to use dose reconstruction and parameter variation to capture and narrow the uncertainty in the derived key parameter values governing the uptake into and transport through the skin. Follow-up case studies on the dermal absorption modelling of BPA are therefore needed to further demonstrate the predictive performance of the MPML MechDermA model and to enhance confidence in the use of such *in silico* methods in chemcial risk assessment. The applicability of the MPML MechDermA model will be further scrutinized in a follow-up paper involving a controlled toxicokinetic study with dermal administration of BPA to the volar forearm (Sasso et al., 2020) and an *in-vitro* study on percutaneous absorption of BPA through human skin (Toner et al., 2018).

4. Conclusions

Physiologically based toxicokinetic (PBPK) modelling plays an increasing role in pharmaceutical and industrial chemical sectors (Laroche et al., 2018). Using BPA as an example, this study explored the

applicability of a sophisticated and comprehensive modelling and simulation platform in the area of industrial chemicals, and revealed benefits and limitations, a main limitation being the extensive data requirements. Based on a human toxicokinetic study and by means of dose reconstruction from urinary excretion, it was possible to successfully develop and partially verify a PBPK model for dermal exposure *via* hand contact to BPA-containing products. Data gaps and ways to overcome them were addressed. The MPML MechDermA model with its multilayer SC structure was able to capture the kinetics at local and systemic levels during the exposure and post-exposure periods, which a simple 3-compartment absorption model was not capable of. Specifically, preferential partitioning of BPA into the SC lipids in combination with the extended SC of palmar skin could explain the delayed and long-lasting transfer of BPA from the SC into the viable epidermis, and then further *via* dermis into systemic circulation. These findings shed light on the role of the SC to act as temporary reservoir for lipophilic chemicals before systemic absorption, which *inter alia* is relevant for the interpretation of human biomonitoring data and for establishing the relationship between external and internal measures of exposure (Clewell et al., 2008).

CRediT authorship contribution statement

Barbara Wiśniowska: Conceptualization, Methodology, Data curation, Investigation, Writing – original draft, Writing – review & editing. **Susanne Linke:** Project administration, Data curation, Writing – review & editing. **Sebastian Polak:** Conceptualization, Writing – review & editing, Supervision. **Zofia Bielecka:** Data curation, Writing – review & editing. **Andreas Luch:** Writing – review & editing. **Ralph Pirow:** Conceptualization, Methodology, Writing – original draft, Writing – review & editing, Visualization, Supervision, Project administration.

Declaration of Competing Interest

The authors declare the following financial interests/personal relationships which may be considered as potential competing interests:

Sebastian Polak and Zofia Bielecka are Certara UK (Simcyp Division) employees. Certara is a developer of the Simcyp platform which was used in the current study.

All other authors declare that they have no known competing financial interests or personal relationships that could have appeared to influence the work reported in this paper.

Data availability

The observed (experimental) data, which were taken from literature, are publically available from the cited publications. Simcyp workspaces of the developed PBPK models are available on request.

Acknowledgements

The present study was financially supported by the German Federal Institute for Risk Assessment (BfR) (grant number 1329-572). The authors would like to thank Moustapha Sy (BfR) for his valuable comments which helped to improve the manuscript.

Appendix A. Supplementary data

Supplementary data to this article can be found online at https://doi.org/10.1016/j.taap.2022.116357.

References

Baker, L.B., 2019. Physiology of sweat gland function: the roles of sweating and sweat composition in human health. Temperature (Austin) 6, 211–259.

Bernier, M.R., Vandenberg, L.N., 2017. Handling of thermal paper: implications for dermal exposure to bisphenol A and its alternatives. PLoS One 12, e0178449.

Biedermann, S., Tschudin, P., Grob, K., 2010. Transfer of bisphenol A from thermal printer paper to the skin. Anal. Bioanal. Chem. 398, 571–576.

Birnbaum, L.S., Bucher, J.R., Collman, G.W., Zeldin, D.C., Johnson, A.F., Schug, T.T., Heindel, J.J., 2012. Consortium-based science: the NIEHS's multipronged, collaborative approach to assessing the health effects of bisphenol A. Environ. Health Perspect. 120, 1640–1644.

Chen, L., Han, L., Saib, O., Lian, G., 2015. In silico prediction of percutaneous absorption and disposition kinetics of chemicals. Pharm. Res. 32, 1779–1793.

Chetty, M., Johnson, T.N., Polak, S., Salem, F., Doki, K., Rostami-Hodjegan, A., 2018. Physiologically based pharmacokinetic modelling to guide drug delivery in older people. Adv. Drug Deliv. Rev. 135, 85–96.

Cho, C.Y., Shin, B.S., Jung, J.H., Kim, D.H., Lee, K.C., Han, S.Y., Kim, H.S., Lee, B.M., Yoo, S.D., 2002. Pharmacokinetic scaling of bisphenol A by species-invariant time methods. Xenobiotica 32, 925–934.

Clewell, H.J., Tan, Y.M., Campbell, J.L., Andersen, M.E., 2008. Quantitative interpretation of human biomonitoring data. Toxicol. Appl. Pharmacol. 231, 122–133.

Danish EPA (Danish Environmental Protection Agency), 2014. Alternative technologies and substances to bisphenol A (BPA) in thermal paper receipts. In: Environmental Project No. 1553. http://www2.mst.dk/Udgiv/publications/2014/03/978-87-93178-20-5.pdf (accessed 12 September 2020).

EC (European Commission), 2003. European Union Risk Assessment Report: 4,4'-Isopropylenediphenol (bisphenol-A). In: 3rd Priority List, Volume 37. European Commission Joint Research Centre, EUR 20843 EN.

EC (European Commission), 2016. Commission Regulation (EU) 2016/2235 of 12 December 2016 Amending Annex XVII to Regulation (EC) no 1907/2006 of the European Parliament and of the Council Concerning the Registration, Evaluation, Authorisation and Restriction of Chemicals (REACH) as regards bisphenol A.

ECB (European Chemicals Bureau), 2003. European Union Risk Assessment Report Methyl acetate. https://echa.europa.eu/documents/10162/c7120cf0-5500-48ec-96b4-a8b5253b86cb (accessed 12 September 2020).

ECHA (European Chemicals Agency), 2015a. Background document to the opinion on the annex XV dossier proposing restrictions on 4.4′-isopropylidenediphenol (bisphenol A; BPA). ECHA, Helsinki. https://echa.europa.eu/documents/10162/d52d2c6b-2f1c-4ddf-bb44-4e3e42ea1820 (accessed 1 January 2020).

ECHA (European Chemicals Agency), 2015b. Committee for Risk Assessment (RAC) Committee for Socio-Economic Analysis (SEAC). Opinion on an Annex XV dossier proposing restrictions on bisphenol A. ECHA, Helsinki. https://www.echa.europa.eu/documents/10162/209030fc-ca4b-4745-97b6-98bfc4d6bdd3 (accessed 3 December 2019).

ECHA (European Chemicals Agency), 2017a. Member State Committee Support Document for Identification of 4,4′-Isopropylidenediphenol (BPA, Bisphenol A) as a Substance of Very High Concern because of its Endocrine Disrupting Properties which Cause Probable Serious Effects to Human Health which Give Rise to an Equivalent Level of Concern to those of CMR and PBT/vPvB Substances. ECHA, Helsinki. https://echa.europa.eu/documents/10162/908badc9-e65d-3bae-933a-3512a9262e59 (accessed 30 December 2019).

ECHA (European Chemicals Agency), 2017b. Substance Evaluation Conclusion as Required by REACH Article 48 and Evaluation Report for 4,4'-Isopropylidenediphenol. ECHA, Helsinki. https://echa.europa.eu/documents/10162/7971ab80-03c9-4d87-e117-e4dbc9cc54d2 (accessed 30 December 2019).

Eckardt, M., Simat, T.J., 2017. Bisphenol A and alternatives in thermal paper receipts - a German market analysis from 2015 to 2017. Chemosphere 186, 1016–1025.

EFSA CEF Panel (EFSA Panel on Food Contact Materials, Enzymes, Flavourings and Processing Aids), 2015. Scientific opinion on the risks to public health related to the presence of bisphenol A (BPA) in foodstuffs. EFSA J. 13, 3978.

EFSA (European Food Safety Authority), Gundert-Remy, U., Bodin, J., Bosetti, C., FitzGerald, R., Hanberg, A., Hass, U., Hooijmans, C., Rooney, A.A., Rousselle, C., Loveren, H.v., Wölfle, D., Barizzone, F., Croera, C., Putzu, C., Castoldi, A.F., 2017. Bisphenol A (BPA) hazard assessment protocol. EFSA Supporting Publications 14, 1354E.

Egawa, M., Hirao, T., Takahashi, M., 2007. In vivo estimation of stratum corneum thickness from water concentration profiles obtained with Raman spectroscopy. Acta Derm. Venereol. 87, 4–8.

Geens, T., Goeyens, L., Kannan, K., Neels, H., Covaci, A., 2012. Levels of bisphenol-A in thermal paper receipts from Belgium and estimation of human exposure. Sci. Total Environ. 435-436C, 30–33.

Gibson, C.R., Lu, P., Maciolek, C., Wudarski, C., Barter, Z., Rowland-Yeo, K., Stroh, M., Lai, E., Nicoll-Griffith, D.A., 2013. Using human recombinant UDP-glucuronosyltransferase isoforms and a relative activity factor approach to model total body clearance of laropiprant (MK-0524) in humans. Xenobiotica 43, 1027–1036.

Heindel, J.J., Newbold, R.R., Bucher, J.R., Camacho, L., Delclos, K.B., Lewis, S.M., Vanlandingham, M., Churchwell, M.I., Twaddle, N.C., McLellen, M., Chidambaram, M., Bryant, M., Woodling, K., Gamboa da Costa, G., Ferguson, S.A., Flaws, J., Howard, P.C., Walker, N.J., Zoeller, R.T., Fostel, J., Favaro, C., Schug, T.T., 2015. NIEHS/FDA CLARITY-BPA research program update. Reprod. Toxicol. 58, 33–44.

Hormann, A.M., Vom Saal, F.S., Nagel, S.C., Stahlhut, R.W., Moyer, C.L., Ellersieck, M.R., Welshons, W.V., Toutain, P.L., Taylor, J.A., 2014. Holding thermal receipt paper and eating food after using hand sanitizer results in high serum bioactive and urine total levels of bisphenol A (BPA). PLoS One 9, e110509.

Hutzler, J.M., Zientek, M.A., 2016. Non-cytochrome P450 enzymes and glucuronidation. In: Wilson, A.G.E. (Ed.), New Horizons in Predictive Drug Metabolism and Pharmacokinetics. The Royal Society of Chemistry, Cambridge, pp. 79–130.

Iooss, B., Lemaître, P., 2015. A review on global sensitivity analysis methods. In: Dellino, G., Meloni, C. (Eds.), Uncertainty Management in Simulation-Optimization of Complex Systems: Algorithms and Applications. Springer US, Boston, MA, pp. 101–122.
Jamei, M., Turner, D., Yang, J., Neuhoff, S., Polak, S., Rostami-Hodjegan, A., Tucker, G., 2009. Population-based mechanistic prediction of oral drug absorption. AAPS J. 11, 225–237.
Jamei, M., Marciniak, S., Edwards, D., Wragg, K., Feng, K., Barnett, A., Rostami-Hodjegan, A., 2013. The simcyp population based simulator: architecture, implementation, and quality assurance. In Silico Pharmacol. 1, 9.
Jonathan, E., 2008. In vivo sweat film layer thickness measured with Fourier-domain optical coherence tomography (FD-OCT). Opt. Laser Eng. 46, 424–427.
Karrer, C., Roiss, T., von Goetz, N., Gramec Skledar, D., Peterlin Masic, L., Hungerbuhler, K., 2018. Physiologically based pharmacokinetic (PBPK) modeling of the bisphenols BPA, BPS, BPF, and BPAF with new experimental metabolic parameters: comparing the pharmacokinetic behavior of BPA with its substitutes. Environ. Health Perspect. 126, 077002.
Krishnan, A.V., Stathis, P., Permuth, S.F., Tokes, L., Feldman, D., 1993. Bisphenol-A: an estrogenic substance is released from polycarbonate flasks during autoclaving. Endocrinology 132, 2279–2286.
Laroche, C., Aggarwal, M., Bender, H., Benndorf, P., Birk, B., Crozier, J., Dal Negro, G., De Gaetano, F., Desaintes, C., Gardner, I., Hubesch, B., Irizar, A., John, D., Kumar, V., Lostia, A., Manou, I., Monshouwer, M., Muller, B.P., Paini, A., Reid, K., Rowan, T., Sachana, M., Schutte, K., Stirling, C., Taalman, R., van Aerts, L., Weissenhorn, R., Sauer, U.G., 2018. Finding synergies for 3Rs - toxicokinetics and read-across: report from an EPAA partners' forum. Regul. Toxicol. Pharmacol. 99, 5–21.
Lassen, C., Mikkelsen, S.H., Brandt, U.K., 2011. Migration of bisphenol A from cash register receipts and baby dummies. In: Survey of Chemical Substances in Consumer Products, No. 110 2011. Danish Ministry of the Environment. http://www2.mst.dk/udgiv/publications/2011/04/978-87-92708-93-9.pdf (accessed 2 December 2019).
Lee, Y., Hwang, K., 2002. Skin thickness of Korean adults. Surg. Radiol. Anat. 24, 183–189.
Li, J.H., Zhou, B.X., Cai, W.M., 2007. The solubility behavior of bisphenol A in the presence of surfactants. J. Chem. Eng. Data 52, 2511–2513.
Liao, C., Kannan, K., 2011. Widespread occurrence of bisphenol A in paper and paper products: implications for human exposure. Environ. Sci. Technol. 45, 9372–9379.
Liu, J., Martin, J.W., 2017. Prolonged exposure to bisphenol A from single dermal contact events. Environ. Sci. Technol. 51, 9940–9949.
Loucks, D.P., van Beek, E., 2017. System Sensitivity and Uncertainty Analysis, Water Resource Systems Planning and Management: An Introduction to Methods, Models, and Applications. Springer International Publishing, Cham, pp. 331–374.
Lunder, S., Andrews, D., Houlihan, J., 2010. BPA coats cash register receipts. https://www.ewg.org/research/bpa-in-store-receipts (accessed 1 January 2020).
Mazur, C.S., Marchitti, S.A., Dimova, M., Kenneke, J.F., Lumen, A., Fisher, J., 2012. Human and rat ABC transporter efflux of bisphenol A and bisphenol A glucuronide: interspecies comparison and implications for pharmacokinetic assessment. Toxicol. Sci. Off. J. Soc. Toxicol. 128, 317–325.
Mendum, T., Stoler, E., VanBenschoten, H., Warner, J.C., 2011. Concentration of bisphenol A in thermal paper. Green Chem. Lett. Rev. 4, 81–86.
Mielke, H., Partosch, F., Gundert-Remy, U., 2011. The contribution of dermal exposure to the internal exposure of bisphenol A in man. Toxicol. Lett. 204, 190–198.
Mitragotri, S., 2003. Modeling skin permeability to hydrophilic and hydrophobic solutes based on four permeation pathways. J. Control. Release 86, 69–92.
Nitsche, J.M., Wang, T.F., Kasting, G.B., 2006. A two-phase analysis of solute partitioning into the stratum corneum. J. Pharm. Sci. 95, 649–666.
Patel, N., Cristea, S., Rose, R., Salem, F., Abduljalil, K., Johnson, T., Jamei, M., Raney, S. G., Zhang, X., Lin, H.-P., Newman, B., Chow, E., Ghosh, P., Fan, J., Fang, L., Polak, S., 2015. Mechanistic modelling of dermal drug absorption using the Simcyp Multi-phase Multi-layer MechDermA model: case study of a transdermal patch formulation of weak base drug timolol. In: Gordon Research Conference – Barrier Function of Mammalian Skin. https://www.certara.com/wp-content/uploads/Resources/Posters/Patel_2015_GRC_timolol.pdf.
Patel, N., Clarke, J.F., Salem, F., Abdulla, T., Martins, F., Arora, S., Tsakalozou, E., Hodgkinson, A., Arjmandi-Tash, O., Cristea, S., Ghosh, P., Alam, K., Raney, S.G., Jamei, M., Polak, S., 2022. Multi-phase multi-layer mechanistic dermal absorption (MPML MechDermA) model to predict local and systemic exposure of drug products applied on skin. CPT Pharmacometrics Syst. Pharmacol. 11, 1060–1084.
Polak, S., Ghobadi, C., Mishra, H., Ahamadi, M., Patel, N., Jamei, M., Rostami-Hodjegan, A., 2012. Prediction of concentration-time profile and its inter-individual variability following the dermal drug absorption. J. Pharm. Sci. 101, 2584–2595.
Polak, S., Mendyk, A., Patel, N., 2018. Combining machine learning and mechanistic modeling approaches to solve real life problems – assessment of the local tissue binding and its influence on the systemic exposure after topical application of drugs. https://www.certara.com/wp-content/uploads/Resources/Posters/Polak-2018-ACOP-binding-skin.pdf.
Puttrevu, S.K., Arora, S., Polak, S., Patel, N.K., 2020. Physiologically based pharmacokinetic modeling of transdermal selegiline and its metabolites for the evaluation of disposition differences between healthy and special populations. Pharmaceutics 12, 942.
R Core Team, 2022. R: A Language and Environment for Statistical Computing. R Foundation for Statistical Computing, Vienna, Austria.
Rhodes, J., Clay, C., Phillips, M., 2013. The surface area of the hand and the palm for estimating percentage of total body surface area: results of a meta-analysis. Br. J. Dermatol. 169, 76–84.
Sarigiannis, D.A., Karakitsios, S.P., Handakas, E., Simou, K., Solomou, E., Gotti, A., 2016. Integrated exposure and risk characterization of bisphenol-A in Europe. Food Chem. Toxicol. 98, 134–147.
Sarkar, D., 2008. Lattice: Multivariate Data Visualization with R. Springer, New York, NY, USA.
Sarkar, D., Andrews, F., 2019. latticeExtra: Extra Graphical Utilities Based on Lattice. https://CRAN.R-project.org/package=latticeExtra.
Sasso, A.F., Pirow, R., Andra, S.S., Church, R., Nachman, R.M., Linke, S., Kapraun, D.F., Schurman, S.H., Arora, M., Thayer, K.A., Bucher, J.R., Birnbaum, L.S., 2020. Pharmacokinetics of bisphenol A in humans following dermal administration. Environ. Int. 144, 106031.
Scheibel, E.G., 1954. Liquid diffusivities. Ind. Eng. Chem. 46, 2007–2008.
Schreder, E., 2010. On the Money: BPA on Dollar Bills and Receipts. http://saferchemicals.org/sc/wp-content/uploads/sites/3/2014/05/OnTheMoneyReport_Final2.pdf.
Schug, T.T., Heindel, J.J., Camacho, L., Delclos, K.B., Howard, P., Johnson, A.F., Aungst, J., Keefe, D., Newbold, R., Walker, N.J., Thomas Zoeller, R., Bucher, J.R., 2013. A new approach to synergize academic and guideline-compliant research: the CLARITY-BPA research program. Reprod. Toxicol. 40, 35–40.
Sharma, R.P., Schuhmacher, M., Kumar, V., 2018. The development of a pregnancy PBPK Model for bisphenol A and its evaluation with the available biomonitoring data. Sci. Total Environ. 624, 55–68.
Shatkin, J.A., Brown, H.S., 1991. Pharmacokinetics of the dermal route of exposure to volatile organic chemicals in water: a computer simulation model. Environ. Res. 56, 90–108.
Shelby, M.D., 2008. NTP-CERHR monograph on the potential human reproductive and developmental effects of bisphenol A. NTP CERHR MON v, vii-ix, 1–64 and passim.
Street, C.M., Zhu, Z., Finel, M., Court, M.H., 2017. Bisphenol-A glucuronidation in human liver and breast: identification of UDP-glucuronosyltransferases (UGTs) and influence of genetic polymorphisms. Xenobiotica 47, 1–10.
Sumner, T., Shephard, E., Bogle, I.D., 2012. A methodology for global-sensitivity analysis of time-dependent outputs in systems biology modelling. J. R. Soc. Interface 9, 2156–2166.
Talreja, P., Kleene, N.K., Pickens, W.L., Wang, T.F., Kasting, G.B., 2001. Visualization of the lipid barrier and measurement of lipid pathlength in human stratum corneum. AAPS PharmSci 3, E13.
Te Biesebeek, J.D., Nijkamp, N.N., Bokkers, B.G.H., Wijnhoven, S.W.P., 2014. General fact sheet: general default parameters for estimating consumer exposure – updated version 2014. In: RIVM Report 090013003/2014.
Teeguarden, J.G., Twaddle, N.C., Churchwell, M.I., Yang, X., Fisher, J.W., Seryak, L.M., Doerge, D.R., 2015. 24-hour human urine and serum profiles of bisphenol A: evidence against sublingual absorption following ingestion in soup. Toxicol. Appl. Pharmacol. 288, 131–142.
ter Burg, W., Bremmer, H.J., van Engelen, J.G.M., 2007. Do-It-Yourself Products Fact Sheet: To assess the risks for the consumer. In: RIVM report 320104007/2007. National Institute for Public Health and the Environment (RIVM), Bilthoven. https://www.rivm.nl/bibliotheek/rapporten/320104007.pdf (accessed 12 September 2020).
Thayer, K.A., Doerge, D.R., Hunt, D., Schurman, S.H., Twaddle, N.C., Churchwell, M.I., Garantziotis, S., Kissling, G.E., Easterling, M.R., Bucher, J.R., Birnbaum, L.S., 2015. Pharmacokinetics of bisphenol A in humans following a single oral administration. Environ. Int. 83, 107–115.
Toner, F., Allan, G., Dimond, S.S., Waechter Jr., J.M., Beyer, D., 2018. In vitro percutaneous absorption and metabolism of bisphenol A (BPA) through fresh human skin. Toxicol. In Vitro 47, 147–155.
Völkel, W., Colnot, T., Csanady, G.A., Filser, J.G., Dekant, W., 2002. Metabolism and kinetics of bisphenol A in humans at low doses following oral administration. Chem. Res. Toxicol. 15, 1281–1287.
von Goetz, N., Pirow, R., Hart, A., Bradley, E., Pocas, F., Arcella, D., Lillegard, I.T.L., Simoneau, C., van Engelen, J., Husoy, T., Theobald, A., Leclercq, C., 2017. Including non-dietary sources into an exposure assessment of the European Food Safety Authority: the challenge of multi-sector chemicals such as bisphenol A. Regul. Toxicol. Pharmacol. 85, 70–78.
Wickham, H., Bryan, J., 2022. readxl: Read Excel Files. https://CRAN.R-project.org/package=readxl.
Yang, J., Jamei, M., Yeo, K.R., Tucker, G.T., Rostami-Hodjegan, A., 2007. Prediction of intestinal first-pass drug metabolism. Curr. Drug Metab. 8, 676–684.
Wiśniowska, B., Linke, S., Polak, S., Bielecka, Z., Luch, A., Pirow, R., 2022. Data on bisphenol A and its metabolites ADME properties for physiologically based pharmacokinetic modelling. Submitted to Data in brief.
Yang, X., Doerge, D.R., Teeguarden, J.G., Fisher, J.W., 2015. Development of a physiologically based pharmacokinetic model for assessment of human exposure to bisphenol A. Toxicol. Appl. Pharmacol. 289, 442–456.
Yau, E., Petersson, C., Dolgos, H., Peters, S.A., 2017. A comparative evaluation of models to predict human intestinal metabolism from nonclinical data. Biopharm. Drug Dispos. 38, 163–186.
Yoshikawa, Y., Hayashi, A., Inai, M., Matsushita, A., Shibata, N., Takada, K., 2002. Permeability characteristics of endocrine-disrupting chemicals using an in vitro cell culture model, Caco-2 cells. Curr. Drug Metab. 3, 551–557.